Multiquasiparticle states in the neutron-rich nucleus ^{174}Tm

R. O. Hughes,[1,*] G. J. Lane,[1] G. D. Dracoulis,[1] A. P. Byrne,[1] P. Nieminen,[1,†] H. Watanabe,[1,‡] M. P. Carpenter,[2] P. Chowdhury,[3] R. V. F. Janssens,[2] F. G. Kondev,[4] T. Lauritsen,[2] D. Seweryniak,[2] and S. Zhu[2]

[1]*Department of Nuclear Physics, Research School of Physics and Engineering, Australian National University, Canberra A.C.T., Australia 0200*

[2]*Physics Division, Argonne National Laboratory, Argonne, Illinois, USA*

[3]*Department of Physics, University of Massachusetts Lowell, Lowell, Massachusetts 01854, USA*

[4]*Nuclear Engineering Division, Argonne National Laboratory, Argonne, Illinois, USA*

(Received 8 March 2013; published 16 July 2013)

Deep inelastic and transfer reactions with an 820-MeV, ^{136}Xe beam and various ytterbium and lutetium targets have been employed to study high-spin structures in the neutron-rich thulium isotopes beyond ^{171}Tm. Results in the doubly odd nucleus, ^{174}Tm, include the identification of numerous new two- and four-quasiparticle intrinsic states including several isomers below 1 MeV, and the observation of the $K^\pi = 4^-$ ground state rotational band populated via direct decay from a $\tau = 153(10)$-μs, $K^\pi = 14^-$ isomer at 2092 keV. The 398-keV, $M1$ transition linking the isomer and ground state band is abnormally fast for a highly forbidden, $\Delta K = 10$ decay. This relative enhancement is explained in terms of mixing of the 13^- level with the nearby 13^- member of a $K^\pi = 8^-$ rotational band, with an interaction strength of V $\approx$ 1.4 keV. Multiquasiparticle calculations are compared with the observed states.

DOI: 10.1103/PhysRevC.88.014311 PACS number(s): 21.10.Re, 21.10.Tg, 23.20.Lv, 27.70.+q

I. INTRODUCTION

The prolate deformed nuclei of the rare-earth region typically have numerous neutron and proton Nilsson states near the Fermi surface with large angular momentum projection on the symmetry axis, K. Consequently, the structure of this region is rich with high-seniority multiquasiparticle states constructed from high-K orbitals. Often, when such high-K multiquasiparticle states arise near or below the yrast line, the de-excitation process is limited to decays toward levels with low-K that can only proceed via high-multipolarity transitions or transitions violating the K selection rule by an order of forbiddenness, $\nu = \Delta K - \lambda$. Such states are termed K isomers due to their unusually long lifetimes.

The neutron-rich, rare-earth region provides an ideal hunting ground for the identification and characterization of such isomers. This fact has been exploited over the last few years in a number of studies utilizing deep inelastic and incomplete fusion reactions with pulsed and chopped beams [1–8]. The present results focus on neutron-rich thulium isotopes ($Z = 69$), and specifically on the odd-odd nucleus, ^{174}Tm. Results on the neighboring odd-A nuclei, ^{173}Tm and ^{175}Tm were recently presented [9], while details on the high-K structure of ^{172}Tm can be found in Ref. [8].

Until now, very little was known about the structure of ^{174}Tm. The ground state spin and parity is assumed to be $K^\pi = 4^-$, from the observation of allowed, unhindered β decay from ^{174}Tm to the two lowest 5^- states in ^{174}Yb [10], as well as from systematics. Chasteler *et al.* [11] studied levels in ^{174}Tm populated in the β decay of ^{174}Er with γ and β spectroscopy. They proposed several levels, but without spin or parity assignments. The results were later confirmed by Becker *et al.* [12], with the added assertion (based on the 0^+ nature of the parent state) that the observed decays might feed a low-lying, $K = 0$ isomer, as opposed to the 4^- ground state. Chakrawarthy *et al.* [13] used γ-ray and conversion-electron spectroscopy in an experiment focused on isolating long-lived isomers, following proton-induced spallation reactions on a tantalum target. They identified a $\tau = 3.3$-s, $K^\pi = 0^+$ isomer at 252 keV in ^{174}Tm. The isomer was observed to decay to a $K^\pi = 3^-$ level at 100 keV via an $E3$ transition and, subsequently, to the $K^\pi = 4^-$ ground state.

The new results presented here include comprehensive information on the high-spin structure of this nucleus (up to about 2 MeV), including the identification of a number of two- and four-quasiparticle intrinsic states. Multiquasiparticle calculations are also presented; these are used to assist in configuration assignments for the various intrinsic states identified in this work.

II. EXPERIMENTAL PROCEDURE

The present experiments were performed at Argonne National Laboratory and utilized deep-inelastic and transfer reactions with an 820-MeV, ^{136}Xe beam. Several targets of ^{175}Lu, ^{176}Lu, ^{174}Yb, and ^{176}Yb were used in the experiments, although most of the results presented here were obtained with the ^{176}Yb target. The beam energy and target thickness of about 6 mg/cm^2 were chosen such that the yields of deep inelastic and transfer reactions were maximized by integrating the beam energy from about 24% above the Coulomb barrier down to the barrier itself. The reaction products were stopped in gold

*Present address: Department of Physics, University of Richmond, 28 Westhampton Way, Richmond VA 23173, USA.

†Present address: Fortum, Power Division, P.O. Box 100, FI-00048 Fortum, Finland.

‡Present address: School of Physics and Nuclear Energy Engineering, Beihang University, Beihang 100191, China.

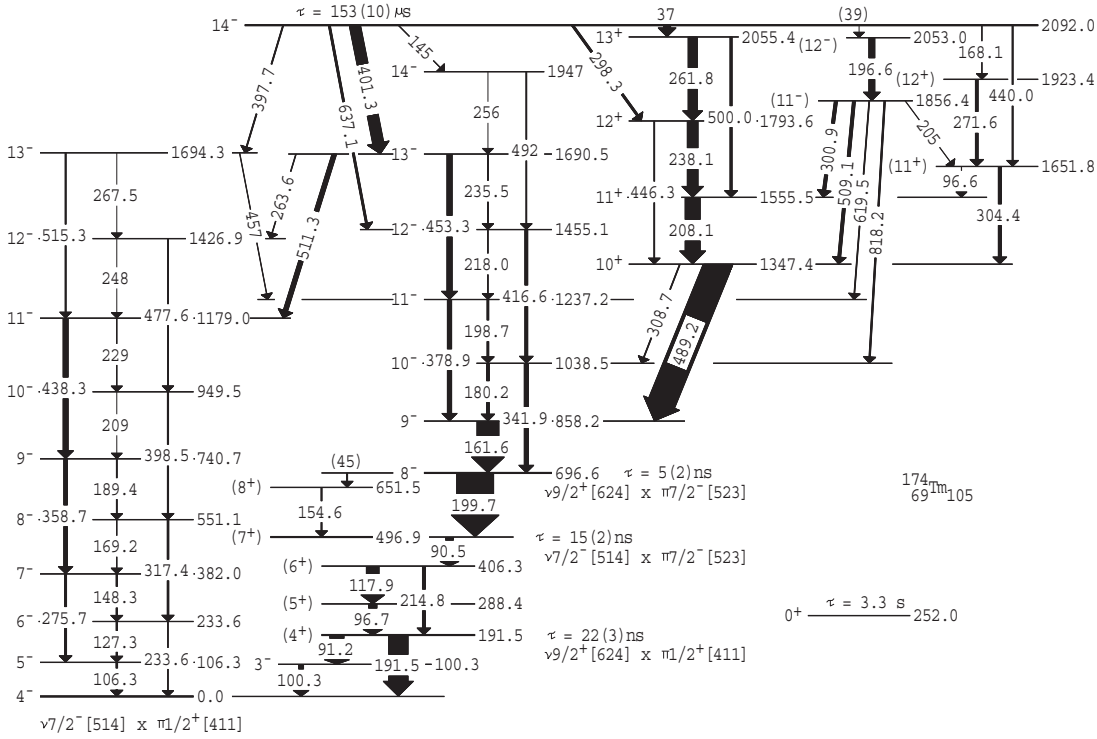

FIG. 1. Proposed level scheme for ^{174}Tm. The 0^+ isomer at 252 keV is from Ref. [13]. Transition thicknesses represent their relative γ-ray intensity.

backings to enable the observation of isomeric decays. The Gammasphere array was used for γ-ray detection with 101 Compton suppressed germanium detectors in operation. The major part of the experiment was performed using a pulsed beam with nanosecond pulses at 825-ns intervals. Data were also collected under different beam-chopping conditions to measure long isomer lifetimes

The γ-ray data were initially sorted into the Blue database [14]. After gain- and time-corrections as well as the removal of detectors with poor timing or resolution, data were selected to construct in-beam (-30 ns to $+100$ ns) and out-of-beam ($+100$ ns to $+750$ ns) γ-γ-γ cubes and other coincidence matrices with various time requirements for analysis with the RADWARE software package [15]. Asymmetric histograms including γ-γ-time-difference and γ-γ-clock cubes were analyzed using software built within ROOT [16].

More detail of the experimental configuration and analysis techniques used in this work can be found in our recent report [9].

III. RESULTS

A partial ^{174}Tm level scheme from the present work is given in Fig. 1. This level structure was initially associated with a thulium isotope through the observation of coincident characteristic x rays. Subsequent assignment to ^{174}Tm was based on the systematic analysis of the relative yield of this structure in measurements using the ^{136}Xe beam, but with different Yb and Lu targets (see Ref. [9]), as well as by the observation of the 100-keV, 3^- state decay identified by Chakrawarthy *et al.* [13]. Transitions reported by Chasteler *et al.* [11] and Becker *et al.* [12] were not seen in the present high-spin study, lending support to the assertion of Becker *et al.*, that the decays might feed a low-lying, low-K isomer. Details leading to the construction of the level scheme are discussed below.

A. Low-lying intrinsic states

Transitions associated with the newly observed 4^- band in ^{174}Tm are presented in a sum of double-gated coincidence spectra in Fig. 2. The band extends up to $J^\pi = 13^-$ where it is fed by a 398-keV transition from a 153-μs isomer placed at 2092 keV.

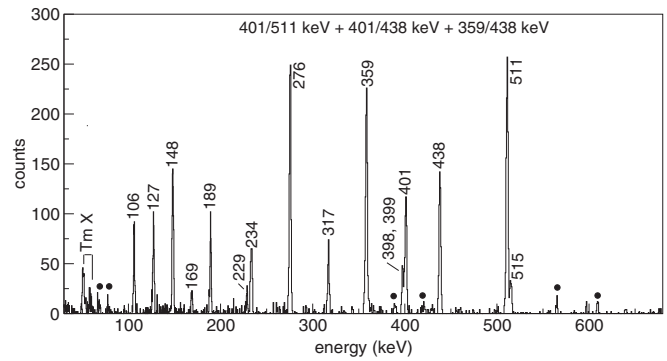

FIG. 2. A γ-ray spectrum obtained from a sum of double-gates in the out-of-beam cube from the ^{176}Yb target data, showing transitions associated with the 4^- rotational band in ^{174}Tm. (Contaminants are labeled with filled circles.)

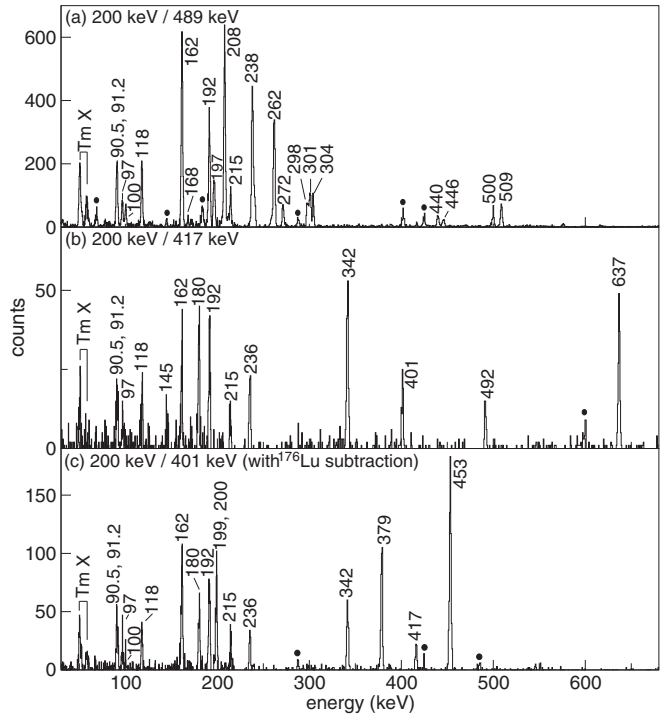

FIG. 3. Coincidence spectra highlighting γ rays associated with ^{174}Tm; (a) Spectrum produced from a double coincidence gate on the 200-/489-keV transitions selecting the most intense decay path fed by the 2092-keV isomer; (b) 200-/417-keV gated spectrum showing the 145-, 401-, and 637-keV transitions which decay from the 2092-keV isomer, and γ rays in the 8^- rotational band; (c) Spectrum produced with a 200-/401-keV double-gate in the ^{176}Yb target data, with the same gate in the ^{176}Lu target data subtracted, to remove a strong ^{176}Lu contaminant.

Figure 3 highlights γ rays associated with several complex cascades that run parallel to the 4^- band. These cascades are also fed by decays from the isomer and pass through several different low-lying intrinsic states that are discussed individually below.

1. 3^- level at 100 keV

The spin and parity quantum numbers for this state were previously established [13]. The associated rotational band has not been observed in the present work.

2. (4^+) isomer at 192 keV

A lifetime of $\tau = 22(3)$ ns for the 192-keV level was obtained from the time-difference spectra of Fig. 4. This newly observed isomer decays by 91.2-keV and 191.5-keV transitions to the 3^- and 4^- bandheads, respectively.

The intensity of the 91.2-keV γ ray was extracted from the combined 90.5-/91.2-keV peak in Fig. 3(a) and balanced against the 100-keV transition intensity, resulting in a measured internal conversion coefficient, $\alpha_T(91.2\ \text{keV}) = 0.63(36)$, to be compared with predictions [17] of 0.43 for an $E1$, 4.04 for an $M1$, 4.38 for an $E2$, and 41.2 for an $M2$ multipolarity. This makes $E1$ the only reasonable assignment for the 91.2-keV transition.

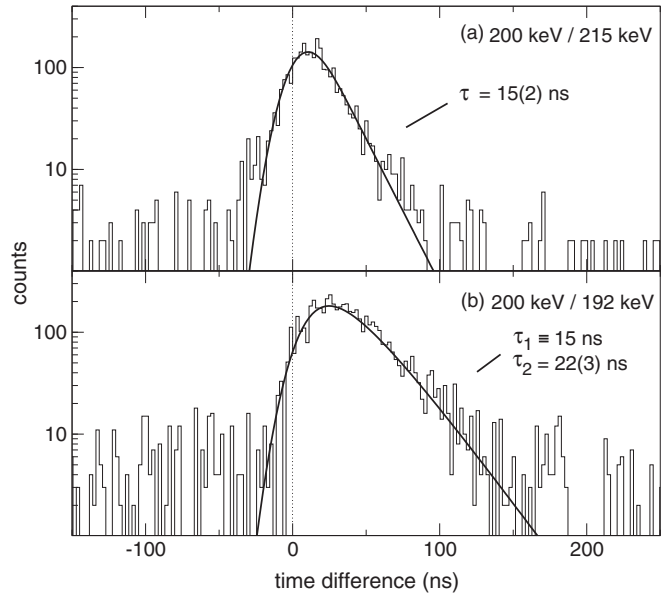

FIG. 4. Time-difference spectra with fits for the 192-keV and 497-keV isomer lifetimes. (a) Spectrum produced by gating on the 200-keV and 215-keV γ rays. A fit gives $\tau = 15(2)$ ns for the 497-keV state. (b) Gate on the 200-keV and 192-keV γ rays where $\tau = 22(3)$ ns is obtained for the 192-keV state lifetime by fixing the 497-keV level lifetime to $\tau = 15$ ns.

The 192-keV branch, also to a negative parity state, must be of $E1$ or $M2$ character. An $M2$ assignment can be ruled out as it would imply an unacceptable [18] transition strength of 90 W.u. The observed $E1$ decays to the 3^- and 4^- states, therefore, limit the spin and parity assignments for the 192-keV level to either 3^+ or 4^+. A 4^+ assignment is favored as no low-lying 3^+ states are expected.

The 97-, 118-, and 215-keV transitions are likely to be part of a band built on the (4^+) level. As discussed below, the rotational alignment and $|g_K - g_R|$ value of this band (Table III) are consistent with predictions for an expected low-lying $K^\pi = 4^+$ state, and, thus, support the present assignments.

3. (7^+) isomer at 497 keV

Figure 4 indicates that the 497-keV state has a lifetime of $\tau = 15(2)$ ns. Balancing the intensities for the 90.5-, 97-, and 215-keV transitions in a 192-/200-keV gated spectrum [taking $\delta(97\ \text{keV}) = 0.27(3)$, deduced assuming $|g_K\text{-}g_R| = 0.50(6)$ from Table II] implies $\alpha_T(90.5\ \text{keV}) = 3.6(6)$, while an intensity balance for the 90.5-keV and 162-keV transitions [taking $\delta(162\ \text{keV}) = 1.2(3)$, deduced assuming $|g_K\text{-}g_R| = 0.10(3)$ for the 8^- band in Table II] gives $\alpha_T(90.5\ \text{keV}) = 3.1(8)$. These values can be compared to predictions [17] of 0.43 for an $E1$, 4.13 for an $M1$, 4.51 for an $E2$, and 42.4 for an $M2$ multipolarity. This suggests a multipolarity of either $M1$ or $E2$ for the 90.5-keV transition. The spin and parity of the 497-keV level is thus limited to $K^\pi = 7^+$ or 8^+. A $K^\pi = (7^+)$ assignment is suggested, since no 8^+ state is expected below 1 MeV in this nucleus, while a low-lying 7^+ state is expected (see discussion below). A 155-keV transition

observed weakly in the out-of-beam data is assigned as the first cascade transition in its related band.

4. 8^- state at 697 keV

A lifetime of $\tau = 5(2)$ ns is deduced for this level from the time-difference spectrum given in Fig. 5(d). The isomer is observed to decay to the 497-keV state via a 200-keV transition, although a weak, unobserved, 45-keV transition to the (8^+), 652-keV level is also inferred from its population in the out-of-beam data. Balancing the total intensity of the 200-keV transition against the 162-keV γ ray in a 91-/489-keV gated spectrum [again assuming $\delta(162\ \text{keV}) = 1.3(3)$] yields $\alpha_T(200\ \text{keV}) = 0.08(4)$. Comparison with predicted values [17] of 0.06 ($E1$), 0.44 ($M1$), 0.26 ($E2$), and 2.37 ($M2$), strongly suggests an $E1$ assignment for the 200-keV transition.

Some of the transitions associated with a rotational band built on this state are evident in Figs. 3(b) and 3(c). The first excited state in this band is populated very strongly by a 489-keV interband transition from the level at 1347 keV. At higher spin, there are strong indications that the 1691-keV member mixes with the 1694-keV, 13^- level of the ground state band, as discussed later. This mixing requires the 1691-keV state to also have $J^\pi = 13^-$, so that the 697-keV bandhead is fixed at $K^\pi = 8^-$. This conclusion also indirectly supports the spin and parity assignments to the low-spin states at 192, 288, 406, 497, and 652 keV.

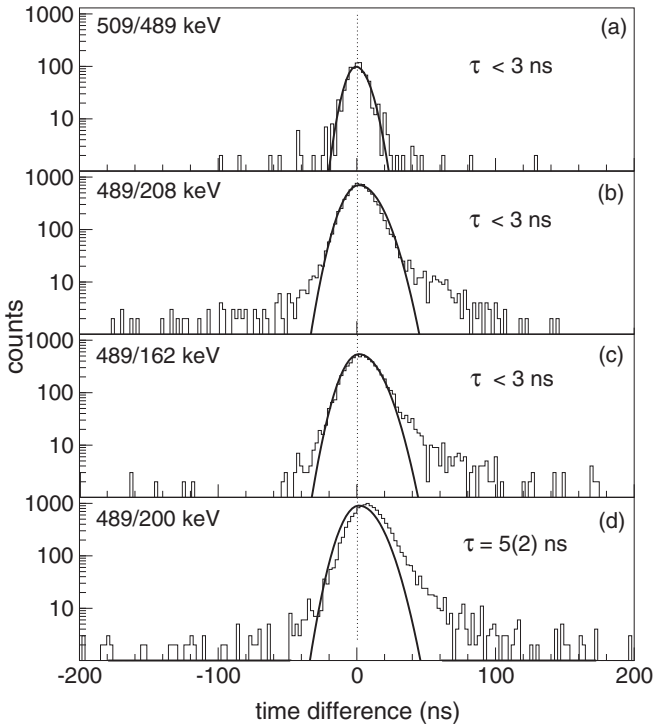

FIG. 5. γ-ray time-difference spectra for transitions in ^{174}Tm. An asymmetric Gaussian prompt response, deduced from transition pairs with comparable energies known to be in prompt coincidence in other isotopes is overlayed in each case. Deviation from the prompt fit indicates a shift due to a short, intervening isomer; (a) 509-/489-keV time difference resulting in $\tau < 3$ ns for the 1347-keV level; (b) 489-/208-keV time difference giving $\tau < 3$ ns for the 1347-keV level; (c) 489-/162-keV time difference leading to $\tau < 3$ ns for the 858-keV level; (d) 489-/200-keV time difference indicating $\tau = 5(2)$ ns for the 697-keV level.

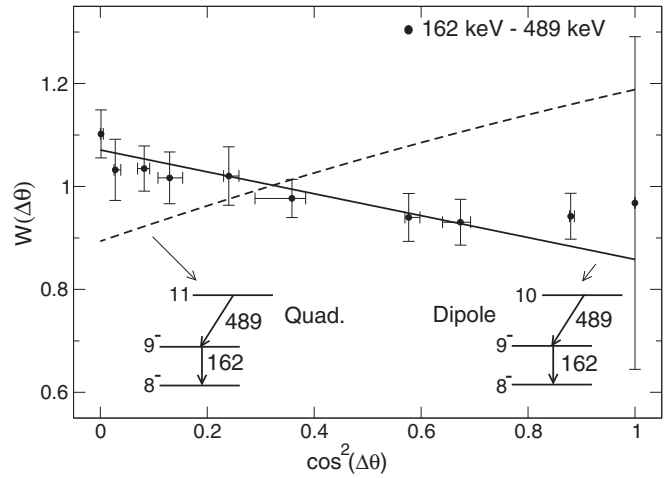

FIG. 6. Angular correlation for the 162/489 keV transitions in ^{174}Tm. Solid and dashed lines correspond to a $J = 10$ or $J = 11$ assignment for the 1347-keV level, respectively.

B. Higher-lying intrinsic states

1. 10^+ state at 1347 keV

The time-difference spectra in Fig. 5(a) and (b) indicate a conservative lifetime limit of $\tau < 3$ ns for the 1347-keV state. This level decays via two branches to the 9^- and 10^- members of the 8^-, 697-keV band. The lifetime limit and absence of other branches constrains the spin and parity to $K^\pi = 10^+$, 10^-, or 11^-. The multipole order of the 489-keV transition was deduced from a measurement of the angular correlation between it and the 162-keV, $E2/M1$ cascade transition [assuming $\delta(162\ \text{keV}) = 1.2(3)$] using a prescription similar to that outlined in Ref. [5]. The resulting correlation, displayed in Fig. 6, implies that the 489-keV γ ray is of dipole ($M1$ or $E1$) character. An $M1$ multipolarity can be excluded because of the absence of an allowed $E2$ transition to the 697-keV level, leaving only an $E1$ assignment for the 489-keV transition. This and the observation of a weaker $E1$ transition to the 10^- level at 1039 keV fixes the spin and parity of the 1347-keV state to $K^\pi = 10^+$.

Transitions associated with the 10^+ rotational band can be seen in the spectra of Figs. 3(a) and 7. The band is populated by 37- and 298-keV transitions from the 14^- isomer. An intensity balance between these two transitions [assuming $\delta(238\ \text{keV}) = 0.29(4)$] in a spectrum gated on the 208- and 262-keV γ rays, results in $\alpha_T(37\ \text{keV}) = 2.5(-1.9,+4.3)$. The large uncertainty originates from the low-intensity of the 37-keV line combined with a 30% uncertainty in the efficiency curve below 60 keV [9]. Comparison with predicted values [17] of 0.9 ($E1$), 9.3 ($M1$), 241 ($E2$), and 609 ($M2$) suggests an $E1$ assignment for the 37-keV transition, although an $M1$ assignment cannot be ruled out. An $E1$ assignment is

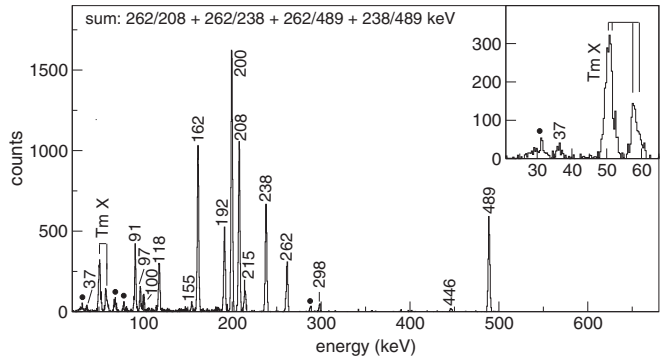

FIG. 7. γ-ray spectrum produced from a sum of double-gates on γ rays in ^{174}Tm. The expanded inset shows the weak, 37-keV transition from the 2092-keV isomer. (Contaminants are labeled with filled circles.) The broad peak at ∼30 keV is most likely a xenon x-ray contaminant from the ^{136}Xe beam.

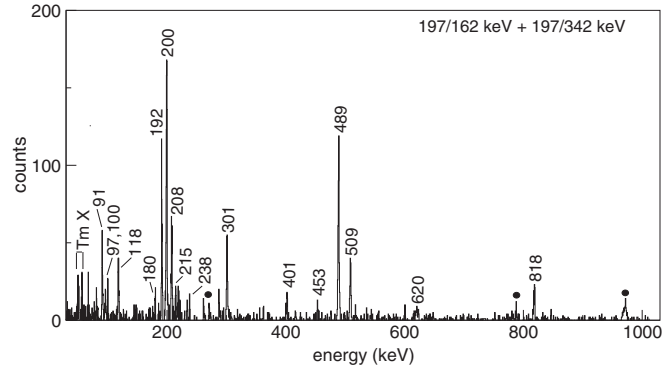

FIG. 8. A spectrum showing γ rays in ^{174}Tm obtained from a sum of 197-/162-keV and 197-/342-keV double-gates. The spectrum shows 301-, 509-, 620-, and 818-keV γ-ray branches from the 1856-keV state. Contaminants are labeled with filled circles.

consistent with the proposed spin and parity assignments and is strongly favored.

2. (11^+) state at 1652 keV

This level deexcites through 304-keV and 96.6-keV γ rays to the 10^+ and 11^+ members of the $K^\pi = 10^+$ band at 1347 keV. A multipolarity assignment for the weak 96.6-keV γ ray requires an intensity balance that accounts for the lower-lying, more intense 96.7-keV transition. Comparison of the resulting $\alpha_T(96.6\ \text{keV}) = 3.1(20)$ value with predictions [17] suggests a possible $M1$ or $E2$ character. However, an $E2$ assignment is excluded since this would imply an $M3$ multipolarity for the 304-keV transition. An $M1$ assignment for the 96.6-keV branch, and a probable $M1$ or $E2$ character for the 304-keV transition restrict the 1652-keV state to $K^\pi = 11^+$ or 12^+. $K^\pi = (11^+)$ is tentatively favored on the basis of hindrance arguments for the 440-keV branch to this state from the 14^- isomer (see discussion below).

3. (12^+) state at 1923 keV

It is unclear whether the 1923-keV level is the first member of the 1652-keV band, or an intrinsic state, since the 272-keV γ ray connecting these levels is higher in energy than the expected energy of 254 keV estimated for the first cascade transition in a $K = 11$ band (assuming $\frac{\hbar^2}{2\mathfrak{J}} = 10.6$ keV). If it is an intrinsic state, the absence of decay branches to states in the 697-keV, 8^- or 1347-keV, 10^+ bands restricts its spin and parity to $J^\pi = 12^+$, 12^-, or 13^+. However, 12^- or 13^+ assignments are unlikely, based on the inspection of the hindrance values for the 168-keV transition from the 2092-keV isomer (see below). A tentative assignment of (12^+) is, therefore, proposed.

4. (11^-) state at 1856 keV

The observation of decay branches of 818, 620, 509, 301, and 205 keV to the 10^- (1039 keV), 11^- (1237 keV), 10^+ (1347 keV), 11^+ (1556 keV), and 11^+ (1652 keV) states, respectively (see Fig. 8), restricts the spin and parity of this level to $K^\pi = 11^\pm$. All five decay branches are thus of dipole character. The 205-, 301-, and 509-keV γ rays to the $K^\pi = 10^+$ and 11^+ bands are allowed, and the 620-keV and 818-keV branches to the $K^\pi = 8^-$ band are twice K-forbidden. An 11^- assignment implies an $E1$ character for the three allowed transitions and an $M1$ multipolarity for the two twice-forbidden decays. Given the intrinsic retardation associated with electric dipole transitions such an assignment seems more likely than the 11^+ alternative. Only an upper lifetime limit of $\tau < 5$ ns was deduced for the 1856-keV level so that the decay strengths could not be measured. The 11^- assignment should therefore be viewed as tentative.

5. (12^-) state at 2053 keV

The 197- and 208-keV transition intensities were balanced [assuming $\delta(208\ \text{keV}) = 0.29(4)$] in a spectrum produced from a double gate on the 301- and 489-keV transitions. The resulting conversion coefficient of $\alpha_T(197\ \text{keV}) = 0.37(13)$ leaves possible $M1$ or $E2$ alternatives for the 197-keV transition from comparison to predictions [17] of 0.06 ($E1$), 0.46 ($M1$), 0.28 ($E2$), and 2.50 ($M2$). The 2053-keV state is, therefore, restricted to $K^\pi = 10^-$, 11^-, 12^-, or 13^-. Spin assignments lower than $J^\pi = 12^-$ are unlikely, since relatively strong decay branches to states in the $K^\pi = 8^-$ band would be expected (as was observed for the decay of the 1856-keV, 11^- state). Furthermore, an assignment of 13^- would make the unobserved, 39-keV transition from the 14^- isomer to this state an allowed $M1$ de-excitation, with a very large hindrance. The state is tentatively assigned as $J^\pi = (12^-)$ on the basis of these considerations. It is possible that the 2053-keV level is the first member of a band built on the $K^\pi = 11^-$, 1856-keV state.

6. 14^- isomer at 2092 keV

The lifetime of the 2092-keV state was measured to be $\tau = 153(10)$ μs from the time curve of Fig. 9. The spectrum was produced from a sum of double gates on strong ^{174}Tm lines in a γ-γ-clock cube constructed from the 1 ms/3 ms chopped data with the ^{176}Yb target (see Ref. [9] for details).

The spin and parity of the isomer can be restricted to $K^\pi = 14^\pm$, based on the observed decay branches to states with firm spin and parity assignments. As will be discussed

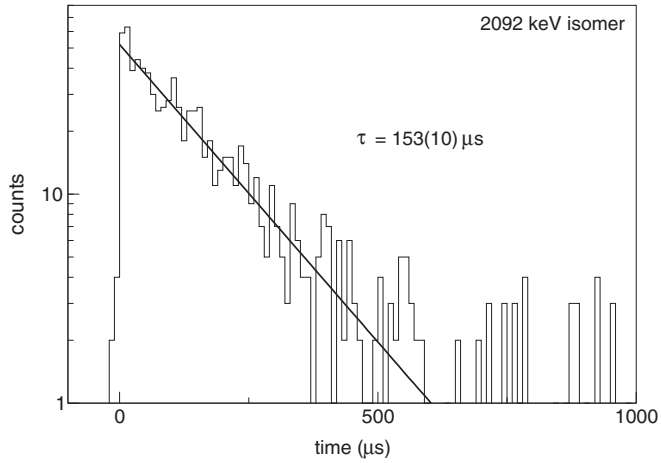

FIG. 9. Decay of the 2092-keV, 14^- isomer in ^{174}Tm as observed in the 1 ms/3 ms-chopped, γ-γ-clock data set obtained with the ^{176}Yb target. The spectrum provides the intensity of coincidence events between the 489-keV transition and the 162-, 200-, and 208-keV γ rays as a function of time. The spectrum was corrected to remove a time distortion at the start of the spectrum, by dividing out nominally flat time spectra produced for the $\tau = 16$ s isomer in ^{176}Yb [19].

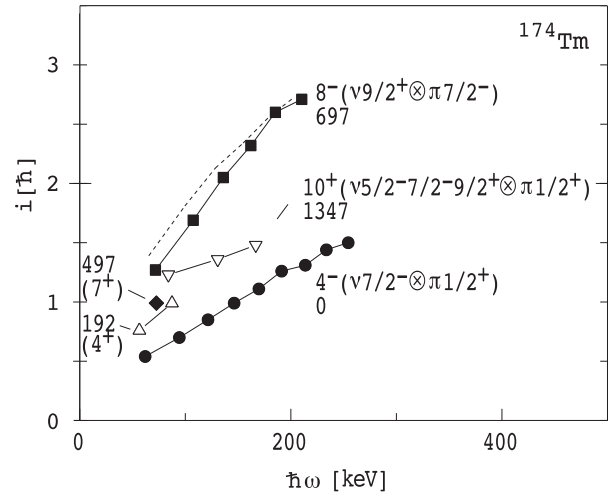

FIG. 10. Net rotational alignment in ^{174}Tm. A reference with Harris parameters of $\Im_0 = 39.5\ \hbar^2$/MeV and $\Im_1 = 50.1\ \hbar^4$/MeV^3 have been subtracted from the observed total alignments. Dashed lines are the sum of empirical neutron and proton alignments that make up a certain multiquasiparticle configuration, as described in the text.

later, negative parity is favored on examination of the reduced hindrances of the isomer branches to the 8^- and 10^+ bands.

Due to the long lifetime, it was not possible to correlate transitions across this isomer. Consequently, levels above the 14^- isomer, including those associated with its rotational band, remain unobserved.

C. Summary of energy levels and γ rays associated with ^{174}Tm

Table I lists the properties of γ-ray transitions assigned to ^{174}Tm, including the energies and intensities, the initial and final level energies, and the spin/parity assignments (where applicable). γ-ray intensities deduced from the out-of-beam data are normalized to the prominent 199.7-keV line. Since there was no single spectrum in which all out-of-beam intensities could be measured, a total feeding intensity is assumed for the 2092-keV isomer, which subsequently feeds down through the decay scheme. The γ-ray intensities from each level are deduced from the total intensity feeding into that level and the measured branching ratios. Conversion coefficients for each γ-ray branch are assumed from Ref. [17]. The intensity errors take into account the uncertainties in conversion coefficients, feeding intensities and branching ratios.

IV. CONFIGURATION ASSIGNMENTS

Due to the degeneracy splitting of parallel and antiparallel couplings of neutron-proton configurations on the one hand, and the fact that neutrons and protons can couple in numerous different configurations on the other, the level density for odd-odd nuclei can be much higher than that for nearby odd-mass nuclei. This makes the level schemes and their interpretation more challenging. Low lying, high-K structures in ^{174}Tm are expected to be formed mainly from the $1/2^+[411]$ and $7/2^-[523]$ proton, and $7/2^-[514]$, $9/2^+[624]$, and $5/2^-[512]$ neutron orbitals.

The rotational alignments of bands in ^{174}Tm are provided in Fig. 10. Reference parameters were taken as the average of the values appropriate for ^{173}Tm and ^{175}Tm. In the figure, the odd-mass reference suggests significant increases in the alignments with increasing spin, even in sequences such as the 4^- ground state band of ^{174}Tm, for which neither the $1/2^+[411]$ proton nor the $7/2^-[514]$ neutron are expected to contribute much rotational alignment. These up-sloping alignments are artificial, arising from the chosen reference parameters which do not take into account a reduced neutron pairing strength due to the unpaired neutron [20,21]. Nevertheless, the present alignment plots are still satisfactory for interpreting the relative alignments of different configurations, but this effect should be kept in mind when examining Fig. 10.

In-band decay properties for rotational bands in ^{174}Tm are displayed in Table II. Table III compares experimentally deduced $|g_K - g_R|$ values with predictions assuming empirical Q_0, g_K, and g_R values adopted from neighboring nuclei [9,22–27].

A. Two-quasiparticle states in ^{174}Tm

1. $\nu\ 7/2^-[514] \otimes \pi\ 1/2^+[411]$ configuration

Previously, the ground state in ^{174}Tm was assigned as the $\nu 7/2^-[514] \otimes \pi 1/2^+[411]$ configuration [10,13], while Chakrawarthy *et al.* [13] proposed that the $K^\pi = 3^-$ excited state at 100 keV was the energetically unfavored, antiparallel coupling of the same configuration. The g factor for the $K^\pi = 4^-$ ground state band is measured to be $|g_K - g_R| = 0.32(6)$ (the weighted average of $|g_K - g_R|$ values from Table II). This measurement compares well to a theoretical prediction of $g_K - g_R = -0.21(6)$ in Table III. It is interesting to note that the rotational energy spacings (and, thus, the implied moment of inertia) of this band are very similar to those observed for the $7/2^-[514]$ ground state band of ^{175}Yb. The implication

TABLE I. Transitions assigned to ^{174}Tm.

E_γ (keV)	I_γ	E_i (keV)	E_f (keV)	K_i^π	J_i^π	K_f^π	J_f^π
37(1)	*373(55)*[b]	2092.0	2055.4	14^-	14^-	10^+	13^+
39(1)[a]	*242(35)*[b]	2092.0	2053.0	14^-	14^-	(12^-)	(12^-)
45(1)[a]	*66(41)*[b]	696.6	651.5	8^-	8^-	(8^+)	(8^+)
90.5(5)	218(56)	496.9	406.3	(7^+)	(7^+)	(4^+)	(6^+)
91.2(6)	393(119)	191.5	100.3	(4^+)	(4^+)	3^-	3^-
96.6(3)	10(7)	1651.8	1555.5	(11^+)	(11^+)	10^+	11^+
96.7(2)	231(59)	288.4	191.5	(4^+)	(5^+)	(4^+)	(4^+)
100.3(3)	138(42)	100.3	0	3^-	3^-	4^-	4^-
106.3(2)	46(14)	106.3	0	4^-	5^-	4^-	4^-
117.9(2)	351(90)	406.3	288.4	(4^+)	(6^+)	(4^+)	(5^+)
127.3(3)	41(13)	233.6	106.3	4^-	6^-	4^-	5^-
145(1)	15(4)	2092.0	1947	14^-	14^-	8^-	14^-
148.3(3)	40(11)	382.0	233.6	4^-	7^-	4^-	6^-
154.6(3)	35(19)	651.5	496.9	(7^+)	(8^+)	(7^+)	(7^+)
161.6(1)	597(133)	858.2	696.6	8^-	9^-	8^-	8^-
168.1(3)	18(5)	2092.0	1923.4	14^-	14^-	(12^+)	(12^+)
169.2(4)	18(6)	551.1	382.0	4^-	8^-	4^-	7^-
180.2(2)	78(25)	1038.5	858.2	8^-	10^-	8^-	9^-
189.4(3)	27(7)	740.7	551.1	4^-	9^-	4^-	8^-
191.5(2)	528(146)	191.5	0	(4^+)	(4^+)	4^-	4^-
196.6(2)	170(25)	2053.0	1856.4	(12^-)	(12^-)	(11^-)	(11^-)
198.7(5)	55(18)	1237.2	1038.5	8^-	11^-	8^-	10^-
199.7(1)	1000(254)	696.6	496.9	8^-	8^-	(7^+)	(7^+)
205(1)	6(3)	1856.4	1651.8	(11^-)	(11^-)	(11^+)	(11^+)
208.1(2)	414(82)	1555.5	1347.4	10^+	11^+	10^+	10^+
209(1)	6(3)	949.5	740.7	4^-	10^-	4^-	9^-
214.8(3)	84(23)	406.3	191.5	(4^+)	(6^+)	(4^+)	(4^+)
218.0(5)	23(9)	1455.1	1237.2	8^-	12^-	8^-	11^-
229(1)	17(4)	1179.0	949.5	4^-	11^-	4^-	10^-
233.6(3)	22(6)	233.6	0	4^-	6^-	4^-	4^-
235.5(4)	25(6)	1690.5	1455.1	8^-	13^-	8^-	12^-
238.1(2)	298(48)	1793.6	1555.5	10^+	12^+	10^+	11^+
248(1)	6(3)	1426.9	1179.0	4^-	12^-	4^-	11^-
256(1)	4(3)	1947	1690.5	8^-	14^-	8^-	13^-
261.8(1)	254(41)	2055.4	1793.6	10^+	13^+	10^+	12^+
263.6(3)	23(6)	1690.5	1426.9	8^-	13^-	4^-	12^-
267.5(5)	5(2)	1694.3	1426.9	4^-	13^-	4^-	12^-
271.6(3)	79(20)	1923.4	1651.8	(12^+)	(12^+)	(11^+)	(11^+)
275.7(1)	59(16)	382.0	106.3	4^-	7^-	4^-	5^-
298.3(2)	65(10)	2092.0	1793.6	14^-	14^-	10^+	12^+
300.9(2)	88(14)	1856.4	1555.5	(11^-)	(11^-)	10^+	11^+
304.4(4)	87(24)	1651.8	1347.4	(11^+)	(11^+)	10^+	10^+
308.7(6)	27(6)	1347.4	1038.5	10^+	10^+	8^-	10^-
317.4(3)	47(15)	551.1	233.6	4^-	8^-	4^-	6^-
341.9(2)	117(37)	1038.5	696.6	8^-	10^-	8^-	8^-
358.7(1)	107(28)	740.7	382.0	4^-	9^-	4^-	7^-
378.9(3)	122(28)	1237.2	858.2	8^-	11^-	8^-	9^-
397.7(3)	34(9)	2092.0	1694.3	14^-	14^-	4^-	13^-
398.5(3)	39(14)	949.5	551.1	4^-	10^-	4^-	8^-
401.3(2)	308(46)	2092.0	1690.5	14^-	14^-	8^-	13^-
416.6(3)	85(29)	1455.1	1038.5	8^-	12^-	8^-	10^-
438.3(1)	141(34)	1179.0	740.7	4^-	11^-	4^-	9^-
440.0(5)	32(8)	2092.0	1651.8	14^-	14^-	(11^+)	(11^+)
446.3(3)	33(5)	1793.6	1347.4	10^+	12^+	10^+	10^+
453.3(3)	147(28)	1690.5	1237.2	8^-	13^-	8^-	11^-
457(1)	14(9)	1694.3	1237.2	4^-	13^-	8^-	11^-
477.6(3)	25(9)	1426.9	949.5	4^-	12^-	4^-	10^-

TABLE I. (*Continued.*)

E_γ (keV)	I_γ	E_i (keV)	E_f (keV)	K_i^π	J_i^π	K_f^π	J_f^π
489.2(1)	756(156)	1347.4	858.2	10^+	10^+	8^-	9^-
492(1)	26(20)	1947	1455.1	8^-	14^-	8^-	12^-
500.0(3)	66(11)	2055.4	1555.5	10^+	13^+	10^+	11^+
509.1(3)	86(14)	1856.4	1347.4	(11^-)	(11^-)	10^+	10^+
511.3(1)	126(24)	1690.5	1179.0	8^-	13^-	4^-	11^-
515.3(3)	30(9)	1694.3	1179.0	4^-	13^-	4^-	11^-
619.5(3)	20(9)	1856.4	1237.2	(11^-)	(11^-)	8^-	11^-
637.1(4)	60(9)	2092.0	1455.1	14^-	14^-	8^-	12^-
818.2(2)	44(9)	1856.4	1038.5	(11^-)	(11^-)	8^-	10^-

[a]Transition unobserved, inferred from coincidence observations.
[b]Total intensity, inferred from intensity balances.

here is that the $1/2^+[411]$ proton coupled to the same neutron in the ^{174}Tm ground state configuration acts as a spectator in terms of the rotational structure.

2. $\nu\, 9/2^+[624] \otimes \pi\ 1/2^+[411]$ configuration

A $K^\pi = 4^+$ state can be produced from a number of alternative configurations, including $\nu 1/2^-[510] \otimes \pi 7/2^-[523]$, $\nu 1/2^-[521] \otimes \pi 7/2^-[523]$, $\nu 7/2^+[633] \otimes \pi 1/2^+[411]$, and $\nu 9/2^+[624] \otimes \pi 1/2^+[411]$. However, given the very low excitation energy for the observed 4^+ isomeric state at 192 keV, all but the (energetically favored) antiparallel coupling of the $\nu 9/2^+[624] \otimes \pi 1/2^+[411]$ configuration can be excluded on the basis that the neutrons involved are located too far from the Fermi level.

Figure 10 indicates that the 192-keV, (4^+) band exhibits slightly more rotational alignment than the 4^- ground state sequence, which is consistent with the presence of an $i_{13/2}$ neutron.

The Gallagher-Moszkowski rules [28] predict that the 5^+ parallel coupling of this configuration will be energetically unfavored and, thus, should lie above the 4^+ coupling. A residual interaction of ± 79 keV was deduced for this configuration using an approach similar to that of Jain *et al.* [29] (including a rotational correction for both states). An expected excitation energy of $E_x \approx 360$ keV is then expected for the 5^+ parallel coupling. No decay branch is observed from the 7^+, 497-keV isomer to this 5^+ state, although it would correspond to an allowed $E2$ transition.

TABLE II. In-band decay properties for rotational bands in ^{174}Tm.

J^π ($\hbar$)	$E_\gamma(M1)$ (keV)	$E_\gamma(E2)$ (keV)	λ $I_{\Delta J=2}/I_{\Delta J=1}$	$\lvert g_K - g_R \rvert$	$\lvert\delta\rvert$
4^-	**0** keV				
6^-	127.3	233.6	0.53(6)	0.37(4)	0.41(5)
7^-	148.3	275.7	1.47(15)	0.33(3)	0.46(5)
8^-	169.2	317.4	2.55(39)	0.32(5)	0.46(7)
9^-	189.4	358.7	4.01(39)	0.31(3)	0.48(5)
10^-	209	398.5	7.7(35)	0.25(11)	0.59(27)
11^-	229	438.3	8.3(14)	0.28(4)	0.52(8)
12^-	248	477.6	4(2)	0.48(23)	0.30(14)
13^-	267.5	515.3	5.8(15)	0.44(11)	0.33(8)
			weighted average 0.32(6)		
4^+	**192 keV**				
6^+	117.9	214.8	0.24(3)	0.50(6)	0.27(3)
8^-	**697 keV**				
10^-	180.2	341.9	1.49(23)	0.07(1)	1.94(29)
11^-	198.7	378.9	2.23(59)	0.11(3)	1.10(29)
12^-	218.0	416.6	3.7(11)	0.11(3)	1.15(32)
13^-	235.5	453.3	6.0(8)	0.09(1)	1.35(18)
14^-	256	492	6.2(56)	0.12(11)	1.03(92)
			weighted average 0.10(3)		
10^+	**1347 keV**				
12^+	238.1	446.3	0.11(1)	0.48(7)	0.29(4)
13^+	261.8	500.0	0.26(3)	0.47(5)	0.30(3)
			weighted average 0.47(7)		

3. $\nu\ 7/2^-[514] \otimes \pi\ 7/2^-[523]$ configuration

Chakrawarthy *et al.* [13] reported a $K^\pi = 0^+$, 252-keV isomer with $\tau = 2.3$ s, that decays to the 3^- state at 100 keV via a 152-keV, $E3$ transition. They suggest that the isomer is the favored, antiparallel coupling of the $\nu\ 7/2^-[514] \otimes \pi\ 7/2^-[523]$ configuration.

The 7^+ level at 497 keV is a good candidate for the energetically unfavored parallel coupling. In the absence of information on its associated rotational band no $\lvert g_K - g_R \rvert$ measurement was possible, but Fig. 10 suggests a reasonably large rotational alignment for the 7^+ band, consistent with the presence of a $h_{11/2}$ proton.

In the odd-odd isotone, ^{176}Lu, an energy difference of 218 keV [30] is seen between the 0^+ and 7^+ couplings of this configuration. This is similar to the difference of 245 keV seen between the 497-keV and 252-keV states in the present case of ^{174}Tm.

4. $\nu\, 9/2^+[624] \otimes \pi\ 7/2^-[523]$ configuration

The observation of a low-lying $7/2^-[523]$ proton excitation (coupled to a $7/2^-[514]$ neutron at 252 keV and 497 keV), and a low-lying $9/2^+[624]$ neutron excitation (coupled to a $1/2^+[411]$ proton at 192 keV), leads to the expectation of a low-lying $\nu\ 9/2^+[624] \otimes \pi\ 7/2^-[523]$ configuration. The 697-keV state is a good candidate for the parallel coupling

TABLE III. Comparison of the experimental $|g_K - g_R|$ and predicted $g_K - g_R$ values for proposed configurations in ^{174}Tm.

K^π	Configuration[a]		$g_K - g_R$[b]	$\lvert g_K - g_R \rvert$
	ν	π	predicted	measured
3^-	$7/2^-[514]$	$\downarrow 1/2^+[411]$	+0.21(8)	
4^-	$7/2^-[514]$	$\uparrow 1/2^+[411]$	−0.21(6)	0.32(6)
4^+	$9/2^+[624]$	$\downarrow 1/2^+[411]$	−0.39(9)	0.50(6)
5^+	$9/2^+[624]$	$\uparrow 1/2^+[411]$	−0.61(7)	
7^+	$7/2^-[514]$	$\uparrow 7/2^-[523]$	+0.45(9)	–
8^-	$9/2^+[624]$	$\uparrow 7/2^-[523]$	+0.12(9)	0.10(3)
10^+	$7/2^-[514]$ $9/2^+[624]$ $5/2^-[512]$	$\downarrow 1/2^+[411]$	−0.35(7)	0.47(7)
11^+	$7/2^-[514]$ $9/2^+[624]$ $5/2^-[512]$	$\uparrow 1/2^+[411]$	−0.45(7)	–
11^-	$7/2^+[633]$ $7/2^-[514]$ $9/2^+[624]$	$\downarrow 1/2^+[411]$	−0.29(7)	–
12^-	$7/2^+[633]$ $7/2^-[514]$ $9/2^+[624]$	$\uparrow 1/2^+[411]$	−0.39(7)	–
14^-	$7/2^-[514]$ $9/2^+[624]$ $5/2^-[512]$	$\uparrow 7/2^-[523]$	−0.07(8)	–

[a]Arrows show the parallel (up) or antiparallel (down) coupling of the quasiproton in the configuration.
[b]g_Ω values are taken from various empirical measurements [9,22–26], the g_R value is taken to be 0.34(2) [27].

of this configuration, and no alternative 8^- configuration is expected at this low energy.

The experimentally deduced value of $|g_K - g_R| = 0.10(3)$ is in excellent agreement with the predicted value of 0.12(9) (Table III), corroborating the configuration assignment. The 1^-, antiparallel coupling is expected to lie at about 770 keV, after allowing for the residual interactions, but is not observed in the present work.

Figure 10 indicates a large rotational alignment for this band, consistent with the presence of both a $h_{11/2}$ proton and an $i_{13/2}$ neutron in the configuration. The dotted line in the figure is a sum of the alignments from the $7/2^-[523]$ proton (from the mean of ^{173}Tm and ^{175}Tm values) and $9/2^+[624]$ neutron (from ^{175}Yb [31,32], taking the average of two references that are appropriate for the ground state bands in ^{174}Yb and ^{176}Yb, respectively). The good agreement lends further support to the proposed configuration assignment.

5. *Hindered decays from the low-lying isomers*

Table IV presents hindrance values for decays from the intermediate isomers at 192, 497, and 697 keV. In the case of the 90.5-keV, $M1$ decay from the 497-keV isomer the transition is K-forbidden ($\nu = 2$), and the corresponding reduced hindrance has a reasonable value of $f_\nu = 42(4)$. The $E1$ transitions associated with the (4^+) and 8^- isomer decays all have strengths that fall close to 10^{-5} W.u.; this seems slightly high (for comparison, allowed $E1$ transitions in ^{173}Tm have strengths around 10^{-6} W.u. [9]). With the present proposed configuration assignments, the decays from both isomers represent the same $9/2^+[624] \rightarrow 7/2^-[514]$ neutron configuration change, coupled to a $1/2^+[411]$ proton in the case of the $(4^+) \rightarrow 3^-$ and $(4^+) \rightarrow 4^-$ decays, and to a $7/2^-[523]$ proton for the $8^- \rightarrow (7^+)$ and $8^- \rightarrow (8^+)$ decays. In the rare-earth region, numerous examples of relatively fast $E1$ transitions associated with the $9/2^+[624] \rightarrow 7/2^-[514]$ neutron configuration change have been observed. It has been proposed that this may be attributed to an octupole softness [33].

B. Four-quasiparticle states in ^{174}Tm

According to the multiquasiparticle calculation (see Table VII below), two-quasiparticle configurations with $K > 9$, as well as six-quasiparticle configurations, will not appear below 2 MeV. The high-K states between 1347 and 2092 keV, therefore, most probably arise from four-quasiparticle configurations. Figure 11 compares $\nu^3 \otimes \pi$ configurations in the odd-odd isotones, ^{176}Lu and ^{178}Ta, with the states observed in ^{174}Tm. Common three-neutron

TABLE IV. Hindrance values for transitions of multipolarity, σL, de-exciting low-lying isomers in ^{174}Tm.

Initial State J^π	E_γ (keV)	I_γ relative	σL	α_T	$B(\sigma L)$[a]	Hindrance F_W
191.5 keV	$\tau = 22(3)$ ns					
(4^+)	91.2	393(119)	$E1$	0.425	$1.32(47) \times 10^{-5}$	$1.52(55) \times 10^5$
	191.5	528(146)	$E1$	0.060	$1.92(66) \times 10^{-6}$	$1.05(36) \times 10^6$
496.9 keV	$\tau = 15(2)$ ns					
(7^+)	90.5	218(56)	$M1$	4.13	$9.97(13) \times 10^{-4}$	$1.80(24) \times 10^3$
696.6 keV	$\tau = 5(2)$ ns					
8^-	199.7	1000(254)	$E1$	0.054	$1.41(68) \times 10^{-5}$	$1.43(68) \times 10^5$
	45	43(27)	$E1$	0.53	$5.3(42) \times 10^{-5}$	$3.8(30) \times 10^4$

[a]$B(E1)$ units are e^2fm^2 and $B(M1)$ units are μ_N^2.

TABLE V. Hindrance values for decay branches from the 2092-keV isomer in ^{174}Tm. The allowed, 39-, 168-, and 440-keV decay information is only given for the adopted 14^- assignment.

E_γ (keV)	I_γ (rel.)	σL	α_T	$B(\sigma L)$[a]	F_W	ν	f_ν
Option (a): 14^+ $\tau = 153(10)$ μs							
398	34(9)	$E1$	0.010	$1.87(53) \times 10^{-12}$	$1.07(30) \times 10^{12}$	9	22(1)
637	60(9)	$M2$	0.058	$2.33(42) \times 10^{-4}$	$2.21(40) \times 10^{5}$	4	22(1)
401	308(46)	$E1$	0.010	$1.65(29) \times 10^{-11}$	$1.22(22) \times 10^{11}$	5	165(6)
145	15(4)	$E1$	0.125	$1.70(48) \times 10^{-11}$	$1.18(33) \times 10^{11}$	5	164(10)
298	65(10)	$E2$	0.073	$1.24(23) \times 10^{-4}$	$4.66(85) \times 10^{5}$	2	683(63)
37	36(5)[b]	$M1$	9.25	$2.23(38) \times 10^{-7}$	$8.0(14) \times 10^{6}$	3	200(12)
Option (b): 14^- $\tau = 153(10)$ μs							
398	34(9)	$M1$	0.068	$1.53(43) \times 10^{-10}$	$1.17(33) \times 10^{10}$	9	13(1)
637	60(9)	$E2$	0.009	$2.33(42) \times 10^{-6}$	$2.48(44) \times 10^{7}$	4	71(3)
401	308(46)	$M1$	0.067	$1.35(24) \times 10^{-9}$	$1.32(24) \times 10^{9}$	5	67(3)
145	15(4)	$M1$	1.07	$1.40(40) \times 10^{-9}$	$1.28(36) \times 10^{9}$	5	66(4)
298	65(10)	$M2$	0.609	$1.01(18) \times 10^{-2}$	$5.07(92) \times 10^{3}$	2	71(7)
37	195(29)[b]	$E1$	0.913	$1.21(22) \times 10^{-8}$	$1.66(30) \times 10^{8}$	3	550(33)
39	1.3(3)[b]	$E2$	186	$5.9(15) \times 10^{-2}$	983(246)	0	–
168	18(5)	$M2$	4.34	$4.9(15) \times 10^{-2}$	1039(306)	0	–
440	32(8)	$E3$	0.076	87.7(24)	21(6)	0	–

[a] $B(EL)$ units are $(e^2\text{fm}^{2L})$ and $B(ML)$ ones are $(\mu_N^2\text{fm}^{2L-2})$.
[b] Intensity inferred from intensity balances.

configurations seen in the higher-mass isotones should also be expected at similar energies (albeit with different proton couplings) in ^{174}Tm, as is implied by the figure.

1. 14^- isomer at 2092 keV

Table V shows reduced hindrance values for the two possible spin and parity assignments of 14^- and 14^+ for the 2092-keV isomer. As will be discussed, the observed strengths favor negative parity. In the case of the $E1$ transitions, for example, while reduced hindrance values are expected to fall within the range $f_\nu \sim$ 30–200 [34,35], $E1$ transitions are normally more retarded (hence, the frequent use of an additional, arbitrary, reduction factor which is not included here) but large variations are observed. In the case of positive parity, the values for the 401- and 145-keV $E1$ transitions are probably abnormally low. In contrast, the high reduced hindrance of 550(33) for the 37-keV $E1$ transition in the case of negative parity seems acceptable. For comparison, $E1$ reduced hindrances of several thousand are observed in ^{172}Tm [8]. The reduced hindrances (≈22) of the 398-keV ($E1$) and 637-keV ($M2$) transitions in the case of positive parity would both be anomalously low. In contrast, the low hindrance observed for the 398-keV transition in the case of negative parity is naturally explained (see below) by mixing of the 1691- and 1694-keV levels. Finally, the very large reduced hindrance for the 298-keV $E2$ transition would be sufficient, by itself, to exclude positive parity.

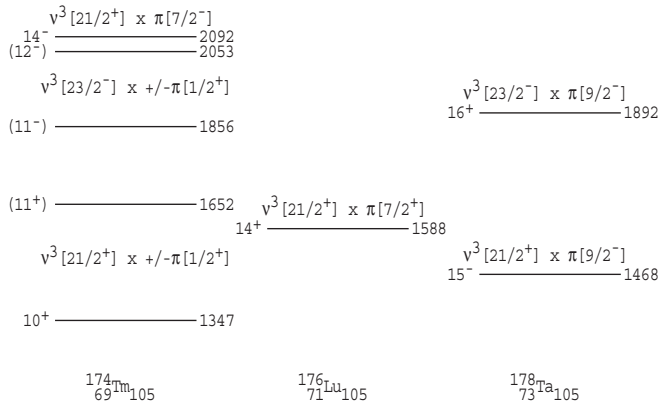

FIG. 11. Multiquasiparticle states in the $N = 105$, odd-odd isotones. Configuration assignments in ^{174}Tm are on the basis of the expected couplings of the three-quasineutron states in the odd-odd neighbors to unpaired $1/2^+[411]$ and $7/2^-[523]$ protons in ^{174}Tm. The proton labels refer to the $1/2^+[411]$, $7/2^-[523]$, $7/2^+[404]$, and $9/2^-[514]$ orbitals. For the neutron labels, $\nu^3[21/2^+]$ represents the $5/2^-[512]7/2^-[514]9/2^+[624]$ configuration and $\nu^3[23/2^-]$ represents the $7/2^+[633]7/2^-[514]9/2^+[624]$ configuration.

An obvious candidate for the configuration of the 14^- isomer (as implied in Fig. 11), is the $\nu 5/2^-[512]7/2^-[514]9/2^+[624]\otimes\pi 7/2^-[523]$ configuration.

2. 1347-keV, 10^+ and 1652-keV, (11^+) states

The experimentally deduced value of $|g_K - g_R| = 0.47(7)$ for the band built on the 1347-keV state is in reasonable agreement (Table III) with the value of $-0.35(7)$ predicted for the antiparallel $1/2^+[411]$ proton, coupled to the $\nu 5/2^-[512]7/2^-[514]9/2^+[624]$ configuration. As no other $K^\pi = 10^+$ states are expected so low in energy, this seems a likely assignment. The large rotational alignment for this band (shown in Fig. 10) is consistent with the presence of an $i_{13/2}$ neutron in the configuration.

The parallel, 11^+, coupling of the $\nu 5/2^-[512]7/2^-[514]9/2^+[624]\otimes\pi 1/2^+[411]$ configuration

TABLE VI. Comparison of neutron-proton residual interactions for two-quasiparticle configurations, as deduced from observations in ^{172}Tm, ^{174}Tm, and ^{175}Tm, with adopted values from Kondev [36].

Configuration		$K^{\pi}_{<}$	E_x	E_{rot}	$K^{\pi}_{>}$	E_x	E_{rot}	E_{res}(exp)	E_{res}(Ref. [36])
ν	π		(keV)	(keV)		(keV)	(keV)	(keV)	(keV)
^{172}Tm									
$5/2^-[512]$	$1/2^+[411]$	2^-	0.0	20.9	3^-	240	33.8	$\mp$115	$\mp$117
$5/2^-[512]$	$7/2^-[523]$	1^+	610.1	10.8	6^+	476.2	64.8	$\pm$94	$\pm$93[a]
^{174}Tm									
$7/2^-[514]$	$1/2^+[411]$	3^-	100.3	31.8	4^-	0.0	42.4	$\pm$55	$\pm$60
$7/2^-[514]$	$7/2^-[523]$	0^+	252.0	0.0	7^+	496.9	74.2	$\mp$45[b]	$\mp$43
^{175}Tm[c]									
$9/2^+[624]$	$1/2^+[411]$	4^+			5^+			$\mp$79[c]	$\mp$70

[a]Taken from average experimental values deduced for ^{166}Ho [37] and ^{168}Ho [38].
[b]Includes a Newby shift [39] of -155.5 keV for the 0^+ coupling of this configuration [40].
[c]This residual interaction was deduced indirectly from a three-quasiparticle configuration in ^{175}Tm [9].

is expected, from the residual interactions (see Table VI below), to be ∼278 keV higher in energy than the antiparallel, 10^+, counterpart assigned to the 1347-keV state. The observed (11^+) state at 1652 keV is 305 keV higher and is a likely candidate for this configuration.

The possibility of an alternative 12^+ assignment for the 1652-keV state would imply that the 440-keV transition from the 14^- isomer to the 1652-keV level is an allowed, $M2$ transition, with a large hindrance of $F_W = 7(2)\times10^4$. A spin and parity of 11^+ is therefore most likely. Table V shows that with the 11^+ assignment, the 440-keV transition is an allowed $E3$ with a hindrance of $F_W = 21(6)$. This hindrance is similar to those of $\pi 7/2^-[523] \rightarrow \pi 1/2^+[411]$, $E3$ transitions observed in the odd-A thulium neighbors [9]. The (11^+) state is thus proposed to arise from the $\nu 5/2^-[512]7/2^-[514]9/2^+[624]\otimes\pi 1/2^+[411]$ configuration.

3. 1923-keV, (12^+) state

The 1923-keV level has possible alternative spins and parities of 12^- or 13^+. While neither can be ruled out, a 12^- assignment would make the 168-keV decay branch from the 14^- isomer an allowed $E2$ transition with a hindrance of $F_W = 1.1(3)\times10^5$. A 13^+ assignment would make the 168-keV γ ray an allowed, $E1$ transition, with a hindrance of $F_W = 1.7(5)\times10^{11}$. In both scenarios, the hindrance values seem unreasonably large. In Table V, a (12^+) assignment for this level leads to the 168-keV transition being of allowed $M2$ character with $F_W = 1039(306)$. This hindrance, while still large, is more reasonable than that implied by the alternative spin and parity assignments. Such a large hindrance value might suggest a transition with a complex configuration change.

There is no obvious assignment for the (12^+), 1923-keV intrinsic state, although a possible candidate is the $\nu 5/2^-[512]7/2^-[514]\,9/2^+[624]\otimes\pi 3/2^+[411]$ configuration given by the multiquasiparticle calculation (see Table VII below). It also remains possible that this state is the (12^+) member of a band built on the (11^+) level at 1652 keV.

4. 1856-keV, (11^-) and 2053-keV, (12^-) states

The (11^-) level is a candidate for the antiparallel coupling of the $1/2^+[411]$ proton with the $\nu 7/2^+[633]7/2^-[514]9/2^+[624]$ three-quasineutron configuration (this state might be expected to be low-lying from Fig. 11). The absence of an associated rotational band means that the assignment cannot be confirmed.

The 12^-, parallel coupling of the same configuration is predicted to occur ∼186 keV above the 11^- coupling (from the residual interactions in Table VI). This is close to the 197-keV gap observed between the 1856- and 2053-keV states. The absence of any other expected 12^- state makes an assignment of the parallel coupling of this configuration to the 2053-keV state seem reasonable.

The 2053-keV state could alternatively have $J^\pi = 13^-$ quantum numbers. The hindrance for the 39-keV, allowed $M1$ transition would then be $F_W = 1.4(4)\times10^7$, which seems to be unreasonably large. For the adopted (12^-) assignment for this level, the 39-keV transition is an allowed $E2$ transition. The corresponding hindrance value of $F_W = 983(246)$ is still large, and could suggest a complex configuration change, where the initial and final state wave functions have little overlap. This might be consistent with the (12^-) state comprising the $\nu 7/2^+[633]7/2^-[514]9/2^+[624]\otimes\pi 1/2^+[411]$ configuration.

V. DISCUSSION

A. Residual nucleon-nucleon interactions

Residual interactions were deduced from the observed energy splittings of the parallel and anti-parallel couplings of the $\nu 5/2^-[512]\otimes\pi 1/2^+[411]$ and $\nu 5/2^-[512]\otimes\pi 7/2^-[523]$ configurations in ^{172}Tm (previously discussed in Ref. [8]), the $\nu 7/2^-[514]\otimes\pi 1/2^+[411]$ and $\nu 7/2^-[514]\otimes\pi 7/2^-[523]$ configurations in ^{174}Tm and the $\nu 9/2^+[624]\otimes\pi 1/2^+[411]$ configuration (indirectly) from ^{175}Tm [9]. These residual interactions are summarized in Table VI. There is generally good agreement with the residual interactions presented in the more comprehensive evaluation of Kondev [36], which were derived in a similar fashion to those presented here.

TABLE VII. Calculated multiquasiparticle states in ^{174}Tm compared to experiment.

K^π	Configuration[a]		E_{qp}	E_{res}	E_{calc}	E_{exp}
	ν	π	(keV)	(keV)	(keV)	(keV)
3^-	$7/2^-$	$1/2^+$	0	+55[b]	110	100
4^-	$7/2^-$	$1/2^+$	0	−55[b]	0[d]	0
0^-	$1/2^-$	$1/2^+$	560	−54[c]	561	
1^-	$1/2^-$	$1/2^+$	560	+57	671	
2^-	$5/2^-$	$1/2^+$	527	−115[b]	467	
3^-	$5/2^-$	$1/2^+$	527	+115[b]	697	
4^+	$9/2^+$	$1/2^+$	233	−79[b]	209	192
5^+	$9/2^+$	$1/2^+$	233	+79[b]	367	
2^-	$7/2^-$	$3/2^+$	626	−70	611	
5^-	$7/2^-$	$3/2^+$	626	+70	751	
3^+	$9/2^+$	$3/2^+$	859	+85	999	
6^+	$9/2^+$	$3/2^+$	859	−85	829	
1^+	$5/2^-$	$7/2^-$	929	+94[b]	1078	
6^+	$5/2^-$	$7/2^-$	929	−94[b]	890	
0^+	$7/2^-$	$7/2^-$	402	−201[b,c]	256	252
7^+	$7/2^-$	$7/2^-$	402	+45[b]	502	497
0^-	$7/2^-$	$7/2^+$	846	+197[c]	1098	
7^-	$7/2^-$	$7/2^+$	846	−128	773	
1^-	$9/2^+$	$7/2^-$	635	+71	761	
8^-	$9/2^+$	$7/2^-$	635	−71	619	697
1^+	$9/2^+$	$7/2^+$	1079	−65	1069	
8^+	$9/2^+$	$7/2^+$	1079	+65	1199	
0^-	$9/2^+$	$9/2^-$	1421	+107[c]	1583	
9^-	$9/2^+$	$9/2^-$	1421	−71	1405	
10^+	$5/2^-, 7/2^-, 9/2^+$	$1/2^+$	1628	−176[b]	1507	1347
11^+	$5/2^-, 7/2^-, 9/2^+$	$1/2^+$	1628	+102[b]	1785	1652
11^-	$7/2^+, 7/2^-, 9/2^+$	$1/2^+$	2023	−79[b]	1999	1856
12^-	$7/2^+, 7/2^-, 9/2^+$	$1/2^+$	2023	+107[b]	2185	(2053)
12^+	$5/2^-, 7/2^-, 9/2^+$	$3/2^+$	2255	−126	2184	(1923)
14^-	$5/2^-, 7/2^-, 9/2^+$	$7/2^-$	2030	−158[b]	1927	2092
14^+	$5/2^-, 7/2^-, 9/2^+$	$7/2^+$	2474	−44	2485	
15^+	$7/2^+, 7/2^-, 9/2^+$	$7/2^-$	2425	−59	2421	
15^-	$5/2^-, 7/2^-, 9/2^+$	$9/2^-$	2817	−142	2730	
18^-	$5/2^-, 7/2^-, 9/2^+$	$1/2^+, 7/2^-, 7/2^+$	3973	−90[b]	3938	
19^+	$5/2^-, 7/2^-, 9/2^+$	$1/2^+, 7/2^-, 9/2^-$	4306	−23[b]	4338	
22^+	$5/2^-, 7/2^-, 9/2^+$	$7/2^-, 7/2^+, 9/2^-$	5425	−368[b]	5112	
23^-	$7/2^+, 7/2^-, 9/2^+$	$7/2^-, 7/2^+, 9/2^-$	5820	−250	5625	

[a]Configurations: (ν) $1/2^-$: $1/2^-[510]$, $7/2^-$: $7/2^-[514]$, $7/2^+$: $7/2^+[633]$, $5/2^-$: $5/2^-[512]$, $9/2^+$: $9/2^+[624]$, $3/2^-$: $3/2^-[512]$. (π) $1/2^+$: $1/2^+[411]$, $7/2^-$: $7/2^-[523]$, $3/2^+$: $3/2^+[411]$, $7/2^+$: $7/2^+[404]$, $9/2^-$: $9/2^-[514]$.

[b]Including residual interactions deduced in Table VI.

[c]$K = 0$ configurations include a Newby shift from Ref. [40].

[d]Energies are increased by 55 keV to account for the fact that the 4^- ground state is depressed in energy due to the residual nucleon interactions.

B. Multiquasiparticle calculations

The model calculations employed here were detailed in Ref. [9]. They use single-particle energies from a Nilsson calculation, some of which were adjusted to approximately reproduce the low-lying single proton and single neutron states observed in the odd-proton and odd-neutron neighbors. The multiquasiparticle pairing calculations use the Lipkin-Nogami formalism (plus pair-blocking). Nucleon-nucleon residual interactions are applied to each configuration to obtain the final calculated energies. These are taken from Table VI where possible and from Ref. [36] in all other cases. The experimental intrinsic states and calculated multiquasiparticle configurations are compared in Table VII, and in Fig. 12. Only multiquasiparticle states reasonably close to the nominal yrast line are included. Note that, in the tables, the shorthand labels used for the neutron and proton Nilsson orbitals are defined in the footnotes.

C. Comparison of experimental and predicted states

The agreement for the two-quasiparticle states is satisfactory. For the four-quasiparticle configurations, the agreement

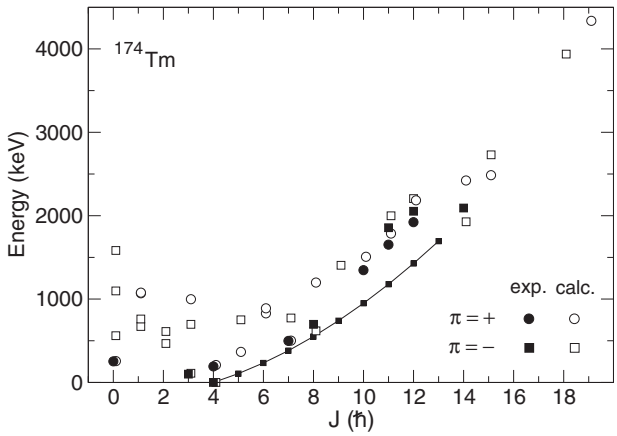

FIG. 12. Calculated and experimental multiquasiparticle state energies for ^{174}Tm. The smaller, filled joined symbols represent the ground state band.

between experiment and the calculations is generally within 150 keV.

The 9^- state from the $\nu 9/2^+[624]\otimes\pi 9/2^-[514]$ configuration is predicted at about 1405 keV, and one might expect branches to its rotational band from the (11^-) state at 1856 keV, although this is not observed experimentally.

The 10^+ and 11^+ couplings of the $\nu 5/2^-[512]7/2^-[514]9/2^+[624]\otimes\pi 1/2^+[411]$ configuration are both predicted about 150 keV higher than observed.

Parallel (12^-) and antiparallel (11^-) couplings of the $\nu 7/2^+[633]7/2^-[514]\,9/2^+[624]\otimes\pi 1/2^+[411]$ configuration are predicted at 2185 keV and 1999 keV, respectively, and may be associated with experimental states observed at 2053 keV (12^-) and 1856 keV, both of which occur ~140 keV below the predicted states.

The $\nu 7/2^+[633]7/2^-[514]9/2^+[624]\otimes\pi 7/2^-[523]$ configuration is calculated to lie at 1927 keV, in reasonable agreement with the 14^- isomer at 2092 keV. The nearest alternative $K = 14$ state is over 500 keV higher in energy.

Predicted low-lying six-quasiparticle states include an 18^- state at 3785 keV and a 22^+ state at 4934 keV (the 22^+ state is not shown in Fig. 12).

D. $\Delta K = 10$ transition from the $K^\pi = 14^-$ isomer to the $K^\pi = 4^-$ band

Table V indicated that the 637-, 401-, and 145-keV transitions to the 8^- band all exhibit reduced hindrances well within the expected range of $f_\nu \sim 30$–200 [34,35]. In contrast, the 398-keV, $M1$ decay to the 13^- member of the ground state band exhibits a very small reduced hindrance of $f_\nu = 13(1)$. The 401-keV transition to the 13^- member of the $K^\pi = 8^-$ band has a similar energy to the relatively enhanced 398-keV decay, and is also of $M1$ multipolarity. However, for the 401-keV γ ray, the observed K change is $\Delta K = 6$, to be compared with $\Delta K = 10$ for the 398-keV transition, i.e., the 398-keV transition is four orders more K-forbidden than the 401-keV decay. Assuming a factor of 100 per degree of K-forbiddenness [34,35], the 398-keV transition would be expected to be about 1×10^8 times weaker than the 401-keV γ ray. In fact, the branching ratio in Table V implies that it is less than ten times weaker.

Figure 13(a) shows the levels of the $K^\pi = 4^-$ and 8^- bands (the ~1983 keV energy for the 14^- member of the 4^- band has been obtained by extrapolation using the rotational model). It is evident that the two bands cross due to the larger alignment associated with the $K^\pi = 8^-$ band. Members of the two bands with the same spin are in close proximity at higher spin values, potentially leading to significant state mixing. Mixing of the 13^- states could specifically lead to an enhancement in the $\Delta K = 10$ transition, as discussed below. It is also possible that the $K^\pi = 14^-$ isomer could mix with the $J^\pi = 14^-$ member of either (or both) of these two bands. For the latter case, the extent of K mixing is governed by the proximity of the states and by the mixing matrix elements. Dracoulis *et al.* [6] showed that the magnitude of the mixing matrix elements associated with K mixing is dependent on the K difference. For $\Delta K = 6$ mixing, a value of $V \sim 100$ eV is expected, while for $\Delta K = 10$ mixing, an upper limit of $V \leqslant 10$ eV is observed empirically. Given the small mixing matrix elements expected and the relatively large energy spacings between the isomer and the 14^- members of the two lower K bands (≈109 keV for the $\Delta K = 10$ case and 145 keV for the $\Delta K = 6$ case), such K mixing is not likely to be significant and it will be neglected in the following calculations.

An expanded image of the two 13^- states and the relevant feeding and decay transitions can be found in Fig. 13(b). The mixing amplitudes of the two 13^- states can be deduced following a procedure similar to that of Refs. [41–43], i.e., by examining the competition of in-band $E2$ and inter-band $E2$ transitions de-exciting the 13^- state at 1691 keV, and separately from the competing $E2$ decays from the 13^- state at 1694 keV. The in-band/interband transition branching ratios are given by the relative transition intensities in Table I. (Note that the reasonable assumption is made that the two bands have the same intrinsic quadrupole moment.) The mixing amplitudes deduced from these calculations are seen to be in good agreement in Table VIII [calculation (a)].

The mixing amplitudes for the 13^- members of the 4^- and 8^- bands can also be deduced independently by comparing the 398-keV and 401-keV transitions from the 14^- isomer to the two 13^- levels. If $\tilde{K}_2$ and $\tilde{K}_3$ are the nominal (mixed) K values of the two 13^- states, the $M1$ matrix elements, in terms

TABLE VIII. Interaction matrix elements, V, and wave function amplitudes for the $J^\pi = 13^-$ members of the $K^\pi = 4^-$ and 8^- bands in ^{174}Tm deduced from (a) the in-band and interband $E2$ branching ratios from the 1691-keV and 1694-keV states, and (b) the intensities of the 398- and 401-keV decays from the 14^- isomer [Eq. (3)].

Transition	(keV)	$\lvert V\rvert$ (keV)	α	β
Calculation (a)				
453.3	511.3	1.4(1)	0.915(16)	0.403(36)
515.3	457	1.5(2)	0.898(40)	0.439(79)
Calculation (b)				
401.3	397.7	1.15(18)	0.947(19)	0.320(57)

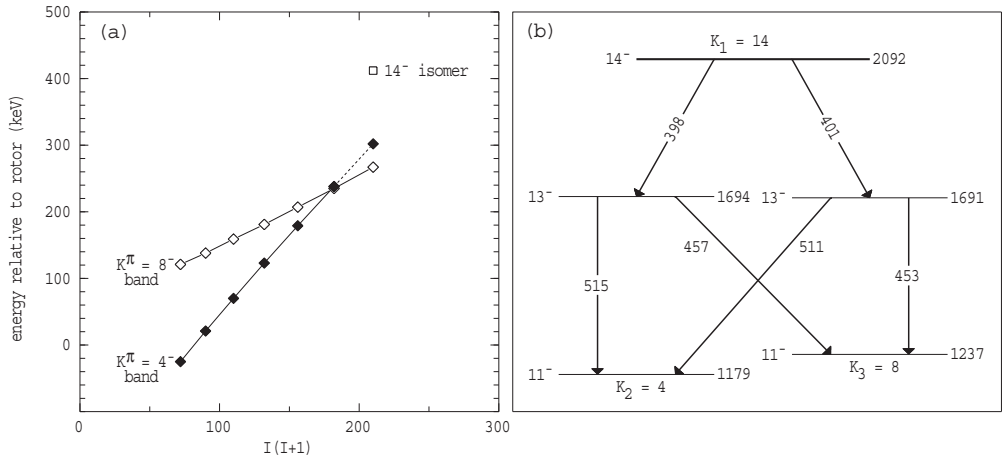

FIG. 13. (a) The $K^\pi = 4^-$ and 8^- bands and 14^- isomer in ^{174}Tm. The unobserved 14^- member of the 4^- band has been obtained by extrapolation. The two bands cross near the $J^\pi = 13^-$ members of the two sequences. (b) Expanded view of the 13^- state mixing scenario in ^{174}Tm.

of the mixing amplitudes, α and β, are given by

$$\begin{aligned}\langle J = 13, \tilde{K}_2 | T(M1) | J = 14, K_1 \rangle \\ = \alpha \langle J = 13, K_2 | T(M1) | J = 14, K_1 \rangle \\ - \beta \langle J = 13, K_3 | T(M1) | J = 14, K_1 \rangle \end{aligned} \quad (1)$$

for the 398-keV transition to the $K_2 = 4$ band, and

$$\begin{aligned}\langle J = 13, \tilde{K}_3 | T(M1) | J = 14, K_1 \rangle \\ = \beta \langle J = 13, K_2 | T(M1) | J = 14, K_1 \rangle \\ + \alpha \langle J = 13, K_3 | T(M1) | J = 14, K_1 \rangle \end{aligned} \quad (2)$$

for the 401-keV transition to the $K_3 = 8$ band. In both cases, the K-value notations are $K_1 = 14$, $K_2 = 4$, and $K_3 = 8$ [as in Fig. 13(b)]. The ($K_1 = 14 \rightarrow K_2 = 4$) transition strength with $\nu = 9$ in both cases should be about 1×10^8 times smaller than the ($K_1 = 14 \rightarrow K_3 = 8$) transition strength with $\nu = 5$ (again, assuming an increase in hindrance of 100 per order of forbiddenness). Neglecting these small $K^\pi = 4^-$ terms, the expected $B(M1)$ value for the 398-keV transition can be written in terms of the 401-keV $B(M1)$ value, according to

$$B(M1; 398) = \frac{\beta^2}{\alpha^2} B(M1; 401), \quad (3)$$

with the additional constraint that $\alpha^2 + \beta^2 = 1$. Taking the experimental transition strengths for the 398-keV and 401-keV transitions from Table V yields values of $\beta = 0.320(57)$ and $\alpha = 0.947(19)$. These amplitudes imply slightly less mixing than those calculated using branching ratios for the in-band and interband $E2$ transitions from the 1691-keV and 1694-keV, 13^- levels (Table VIII), but essentially agree within error.

A corrected reduced hindrance value for the 398-keV transition can be deduced using the amplitudes calculated above (again, the contribution of the $\nu = 9$ component to the transition strength is neglected). Using the mixing amplitudes deduced from the $13^- \rightarrow 11^-$, $E2$ branching ratios, a reduced hindrance of $f_\nu = 96$ is deduced, while using the amplitudes derived from Eq. (3), a value of $f_\nu = 105$ is found. These are acceptable reduced hindrance values, indicating that mixing of the 13^- states with an interaction of $V \sim 1.4$ keV accounts for the relatively enhanced 398-keV transition. This interaction strength is consistent with other cases of K mixing for $\Delta K = 4$ [6].

VI. SUMMARY

Deep-inelastic reactions with a ^{136}Xe beam and various targets including ^{176}Yb have been utilized to probe the high-spin structure in the odd-odd nucleus, ^{174}Tm. The new results identify a number of multiquasiparticle intrinsic states, including several isomers, whose energies are well reproduced in multiquasiparticle calculations. Prior to this work, the structural information on this nucleus was scarce, with only a few intrinsic states identified. The results include identification of the ground state, $K^\pi = 4^-$ rotational band up to spin 13^-. The associated $|g_K - g_R|$ value measured for this band corroborates the $\nu 7/2^-[514] \otimes \pi 1/2^+[411]$ configuration assignment to the ground state. A four-quasiparticle, $K^\pi = 14^-$ isomer has also been identified at 2092 keV with a lifetime of $\tau = 153(10)$ μs. It decays via a fast $\Delta K = 10$ transition to the 13^- member of the ground state band. The relative enhancement of this decay can be attributed to mixing of the 13^- level with the nearby 13^- rotational member of a $K^\pi = 8^-$ band with an interaction of $V \sim 1.4$ keV.

ACKNOWLEDGMENTS

This work was supported through the Australian Research Council Discovery Project No. DP0345844, and by the US Department of Energy, Office of Nuclear Physics, under Contract No. DE-AC02-06CH1135.

[1] G. J. Lane *et al.*, Phys. Rev. C **82**, 051304(R) (2010).
[2] F. G. Kondev, G. D. Dracoulis, A. P. Byrne, T. Kibédi, and S. Bayer, Nucl. Phys. A **617**, 91 (1997).
[3] G. D. Dracoulis *et al.*, Phys. Lett. B **635**, 200 (2006).
[4] G. D. Dracoulis *et al.*, Phys. Rev. C **79**, 061303(R) (2009).
[5] G. D. Dracoulis *et al.*, Phys. Rev. C **71**, 044326 (2005).

[6] G. D. Dracoulis *et al*., Phys. Rev. Lett. **97**, 122501 (2006).
[7] T. R. McGoram, G. D. Dracoulis, T. Kibédi, A. P. Byrne, R. A. Bark, A. M. Baxter, and S. M. Mullins, Phys. Rev. C **62**, 031303(R) (2000).
[8] R. O. Hughes, G. J. Lane, G. D. Dracoulis, T. Kibédi, P. Nieminen, and H. Watanabe, Phys. Rev. C **77**, 044309 (2008).
[9] R. O. Hughes *et al*., Phys. Rev. C **86**, 054314 (2012).
[10] N. Kaffrell and W. Kurcewicz, Nucl. Phys. A **255**, 339 (1975).
[11] R. M. Chasteler, J. M. Nitschke, R. B. Firestone, K. S. Vierinen, P. A. Wilmarth, and A. A. Shihab-Eldin, Z. Phys. A **332**, 239 (1989).
[12] K. Becker, F. Meissner, W.-D. Schmidt-Ott, U. Bosch, V. Kunze, H. Salewski, R. Kirchner, O. Klepper, E. Roeckl, D. Schardt, and K. Rykaczewski, Nucl. Phys. A **522**, 557 (1991).
[13] R. S. Chakrawarthy *et al*., Phys. Rev. C **73**, 024306 (2006).
[14] M. Cromaz, T. J. M. Symons, G. J. Lane, I. Y. Lee, and R. W. Macleod, Nucl. Instrum. Methods, Phys. Res. A **462**, 519 (2001).
[15] D. C. Radford, Nucl. Instrum. Methods, Phys. Res. A **361**, 297 (1995).
[16] Rene Brun and Fons Rademakers, Nucl. Instrum. Methods Phys. Res. A **389**, 81 (1997).
[17] T. Kibédi, T. W. Burrows, M. B. Trzhaskovskaya, P. M. Davidson, and C. W. Nestor, Jr., Nucl. Instrum. Methods Phys. Res. A **589**, 202 (2008).
[18] J. K. Tuli, Nucl. Data. Sheets **94**, 3 (2001).
[19] J. Kantele, Phys. Lett. **2**, 293 (1962).
[20] G. D. Dracoulis, Proceedings of the International Conference on Nuclear Structure at the Limits, Argonne National Laboratory, ANL/PHY-97/148-153 (1996).
[21] G. D. Dracoulis, F. G. Kondev, and P. M. Walker, Phys. Lett. B **419**, 7 (1998).
[22] J. Kern and G. L. Struble, Nucl. Phys. A **286**, 371 (1977).
[23] V. S. Shirley, Nucl. Data Sheets **75**, 377 (1995).
[24] M. S. Basunia, Nucl. Data Sheets **102**, 719 (2004).
[25] F. G. Kondev, Nucl. Data Sheets **98**, 801 (2003).
[26] M. L. Bissell *et al*., Phys. Lett. B **645**, 330 (2007).
[27] A. E. Stuchbery, Nucl. Phys. A **589**, 222 (1995).
[28] C. J. Gallagher, Jr. and S. A. Moszkowski, Phys. Rev. **111**, 1282 (1958).
[29] K. Jain, O. Burglin, G. D. Dracoulis, B. Fabricius, N. Rowley, and P. M. Walker, Nucl. Phys. A **591**, 61 (1995).
[30] M. S. Basunia, Nucl. Data Sheets **107**, 791 (2006).
[31] G. D. Dracoulis *et al*. (unpublished).
[32] N. J. Ncapayi, S. M. Mullins, M. Benatar, E. Gueorgueiva, J. J. Lawrie, G. K. Mabala, S. Mukherjhee, S. H. T. Murray, K. P. Mutshena, R. T. Newman, J. F. Sharpey-Schafer, F. D. Smit, and P. Vymers, Eur. Phys. J. A **26**, 265 (2005).
[33] G. B. Hagemann, I. Hamamoto, and W. Satuła, Phys. Rev. C **47**, 2008 (1993).
[34] L. I. Rusinov, Usp. Fiz. Nauk. **73**, 615 (1961).
[35] K. E. G. Löbner, in *The Electromagnetic Interaction in Nuclear Spectroscopy*, edited by W. D. Hamilton (North Holland, Amsterdam, 1975), p. 141.
[36] F. G. Kondev, Ph.D. thesis, Australian National University, 1996.
[37] D. M. Headly, R. K. Sheline, P. C. Sood, R. W. Hoff, I. Hrĭvnácová, J. Kvasil, D. Nosek, A. K. Jain, and D. G. Burke, At. Data Nucl. Data Tables **69**, 239 (1998).
[38] R. M. Chasteler, J. M. Nitschke, R. B. Firestone, K. S. Vierinen, and P. A. Wilmarth, Phys. Rev. C **42**, R1796 (1990).
[39] N. D. Newby, Jr., Phys. Rev. **125**, 2063 (1962).
[40] A. K. Jain, R. K. Sheline, D. M. Headly, P. C. Sood, D. G. Burke, I. Hrĭvnácová, J. Kvasil, D. Nosek, and R. W. Hoff, Rev. Mod. Phys. **70**, 843 (1998).
[41] E. M. Beck, J. C. Bacelar, M. A. Delaplanque, R. M. Diamond, F. S. Stephens, J. E. Draper, B. Herskind, A. Holm, and P. O. Tjøm, Nucl. Phys. A **464**, 472 (1987).
[42] H. J. Jensen *et al*., Z. Phys A **340**, 351 (1991).
[43] G. J. Lane, Ph.D. thesis, Australian National University, 1995.